

TABLE OF CONTENTS

	Page
ACKNOWLEDGMENTS	iii
ABSTRACT (ENGLISH)	iv
ABSTRACT (THAI)	v
LIST OF TABLES	ix
LIST OF FIGURES	xi
CHAPTER 1 INTRODUCTION	1
1.1 Overview	1
1.2 Purpose of the research	2
CHAPTER 2 LITERATURE REVIEW	4
2.1 Ferroelectric properties and BaTiO ₃	4
2.2 Ferroelectric hysteresis measurement	8
2.3 Ising model	9
2.4 Mean field theory	11
2.4.1 Dynamic mean field equation	12
2.5 Monte Carlo simulation	13
2.5.1 Important sampling	14
2.5.2 Markov process	14
2.5.3 Metropolis algorithm	15

	Page
2.6 Fourier transformation	16
2.6.1 Continuous Fourier transformation	17
2.6.2 Discrete Fourier transformation	18
2.6.3 Fast Fourier transformation	19
CHAPTER 3 METHODOLOGY	24
3.1 Procedure of the research	24
3.2 Ferroelectric hysteresis data	25
3.2.1 Mean field calculation	26
3.2.1 Monte Carlo simulation	27
3.2.3 Sawyer-Tower experiment	28
3.3 Ferroelectric hysteresis properties	33
3.2.1 Hysteresis area	33
3.2.1 Remnant polarization	34
3.2.3 Coercive field	35
3.4 Fourier analysis of ferroelectric hysteresis	35
CHAPTER 4 RESULTS AND DISCUSSIONS	37
4.1 Fourier spectrum characteristic	37
4.2 The relationship between hysteresis properties and amplitude of Fourier harmonics	47
4.2.1 Hysteresis area	47
4.2.2 Remnant polarization	55

	Page
4.2.3 Coercive field	62
4.3 The relationship between external perturbation parameters and amplitude of Fourier harmonics	69
CHAPTER 5 CONCLUSIONS	71
5.1 Conclusions	71
5.2 Suggestions	72
REFERENCES	73
APPENDIX	78
VITA	94

ลิขสิทธิ์มหาวิทยาลัยเชียงใหม่
Copyright© by Chiang Mai University
All rights reserved

LIST OF TABLES

Table	Page
2.1 The number of multiplications of complex number comparison between the discrete Fourier transformation (DFT) and the fast Fourier transformation (FFT).	23
4.1 The hysteresis area ($A_k^{real\ part}$) re-calculated from inverse Fourier transformation of the amplitude of odd k^{th} harmonic of real part (A_k) for Ising hysteresis from mean field calculation in Fig. 4.1 (a).	48
4.2 The hysteresis area ($A_k^{real\ part}$) re-calculated from inverse Fourier transformation of the amplitude of odd k^{th} harmonic of real part (A_k) for Ising hysteresis from Monte Carlo simulation in Fig. 4.1 (b).	50
4.3 The hysteresis area ($A_k^{real\ part}$) re-calculated from inverse Fourier transformation of the amplitude of odd k^{th} harmonic of real part (A_k) for BaTiO ₃ hysteresis from Sawyer-Tower experiment in Fig. 4.1 (c).	52
4.4 The remnant polarization $P_{r_k}^{real\ part}$ re-calculated from inverse Fourier transformation of the amplitude of odd k^{th} harmonic of real part (A_k) for Ising hysteresis from mean field calculation in Fig. 4.1 (a).	55

- 4.5 The remnant polarization $P_{r_k}^{real\ part}$ re-calculated from inverse Fourier transformation of the amplitude of odd k^{th} harmonic of real part (A_k) for Ising hysteresis from Monte Carlo simulation in Fig. 4.1 (b). 57
- 4.6 The remnant polarization $P_{r_k}^{real\ part}$ re-calculated from inverse Fourier transformation of the amplitude of odd k^{th} harmonic of real part (A_k) for BaTiO₃ hysteresis from Sawyer-Tower experiment in Fig. 4.1 (c). 59
- 4.7 The phase-angles φ_k that the combination of polarizations re-calculated from inverse Fourier transformation of the amplitude of odd k^{th} harmonic of real part (A_k) and imaginary (B_k) part are cancelled for Ising hysteresis from mean field calculation in Fig. 4.1 (a). 63
- 4.8 The phase-angles φ_k that the combination of polarizations re-calculated from inverse Fourier transformation of the amplitude of odd k^{th} harmonic of real part (A_k) and imaginary (B_k) part are cancelled for Ising hysteresis from Monte Carlo simulation in Fig. 4.1 (b). 64
- 4.9 The phase-angles φ_k that the combination of polarizations re-calculated from inverse Fourier transformation of the amplitude of odd k^{th} harmonic of real part (A_k) and imaginary (B_k) part are cancelled for BaTiO₃ hysteresis from Sawyer-Tower experiment in Fig.4.1 (c). 66

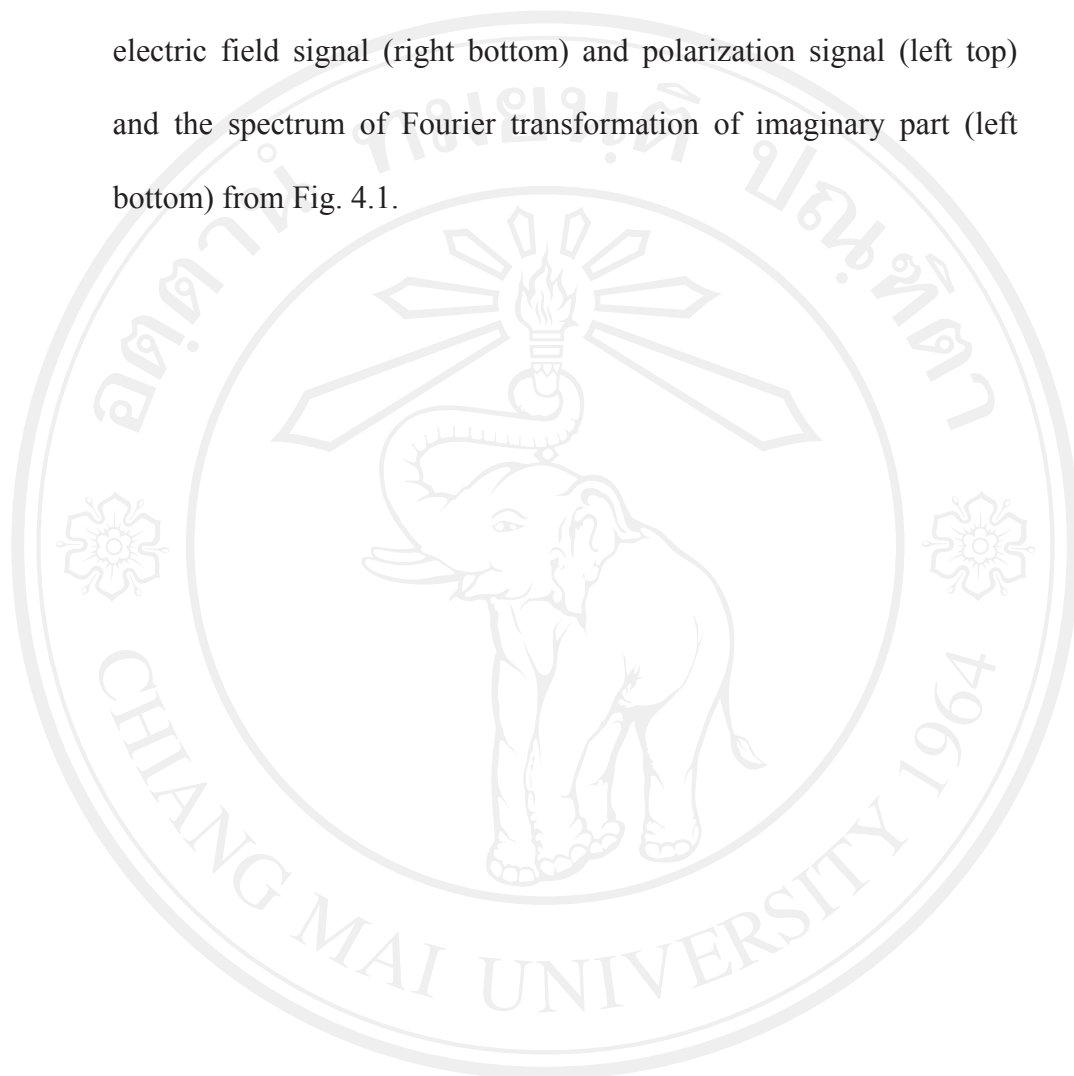
LIST OF FIGURES

Figure	Page
2.1 The classification of crystal structures showing the division into piezoelectric, pyroelectric and ferroelectric materials (modified from [18]).	5
2.2 The transition between paraelectric (a) and ferroelectric (b) phases [19].	6
2.3 Typical ferroelectric hysteresis loop [20].	7
2.4 Perovskite structure of BaTiO ₃ [19].	8
2.5 The temperature dependent crystal structure of BaTiO ₃ [21].	8
2.6 Sawyer-Tower circuit [22, 23].	9
2.7 Ising dipole moments configuration, where each Ising dipole moment u_i (white) interacts mostly with its nearest neighbors u_j (gray).	10
2.8 Butterfly diagram of the fast Fourier transformation by dividing and rearranging data points in 1 step for $N = 8$ (modified from [30]).	21
2.9 Butterfly diagram of the fast Fourier transformation by dividing and rearranging data points in 2 steps for $N = 8$ (modified from [30]).	22
3.1 The research procedure.	25
3.2 The averaging of polarizations having the same electric field data obtained from many hysteresis loops where the target number of data points per period is $N = 32$.	30

- 3.3 The arranging of electric field and its corresponding polarization data relative to the perfect sine waveform having the same electric field amplitude and frequency where the target number of data points per period is $N = 32$. 31
- 3.4 The Loess smoothing of polarization data where the target number of data points per period is $N = 32$. 32
- 3.5 The Cubic spline interpolation of electric field and its corresponding polarization data where the target number of data points per period is $N = 32$. 33
- 4.1 The ferroelectric hysteresis (right top) with its corresponding electric field signal (right bottom) and polarization signal (left top), and the spectrum of Fourier transformation (left bottom) for (a) Ising Ferroelectric hysteresis data from mean field calculation that generated at $T = 2.50 J/k_B$, $E_0 = 4.00 J$ and $f = 0.01 \tau^{-1}$, (b) Ising Ferroelectric hysteresis data from Monte Carlo simulation that generated at $T = 2.00 J/k_B$, $E_0 = 4.00 J$ and $f = 0.01 mcs^{-1}$, and (c) BaTiO₃ Ferroelectric hysteresis data from Sawyer-Tower experiment that measured at $T = 25 \text{ }^\circ\text{C}$, $E_0 = 10 \text{ kV/cm}$ and $f = 10 \text{ Hz}$. 39
- 4.2 The ferroelectric hysteresis (right top) re-calculated from inverse Fourier transformation of the real part with its corresponding electric field signal (right bottom) and polarization signal (top left) and the spectrum of Fourier transformation of real part (left bottom) from Fig. 4.1. 45

4.3 The ferroelectric hysteresis (right top) re-calculated from inverse Fourier transformation of the imaginary part with its corresponding electric field signal (right bottom) and polarization signal (left top) and the spectrum of Fourier transformation of imaginary part (left bottom) from Fig. 4.1.

47



ลิขสิทธิ์มหาวิทยาลัยเชียงใหม่
Copyright© by Chiang Mai University
All rights reserved